Measurement and calculation of absolute cross sections for excitation of the $3s^23p\ ^2P^o_{1/2} - 3s^23p\ ^2P^o_{3/2}$ fine-structure transition in Fe^{13+}

S. Hossain,[1] S. S. Tayal,[2] S. J. Smith,[1] J. C. Raymond,[3] and A. Chutjian[1]
[1]*Jet Propulsion Laboratory, California Institute of Technology, Pasadena, California 91109, USA*
[2]*Department of Physics, Clark Atlanta University, Atlanta, Georgia 30314, USA*
[3]*Harvard-Smithsonian Center for Astrophysics, Cambridge, Massachusetts 02138, USA*
(Received 17 November 2006; published 12 February 2007)

Experimental cross sections are reported for the Fe^{13+} coronal green line transition $3s^23p\ ^2P^o_{1/2} - 3s^23p\ ^2P^o_{3/2}$ at λ5303 Å (2.338 eV). The center-of-mass interaction energies are in the range 1.7 eV (below threshold) through threshold, to 6.6 eV (2.9×threshold). Data are compared with results of a 135-level Breit-Pauli *R*-matrix theory. Present experiment detects a strong maximum in the excitation cross section of magnitude 15×10^{-16} cm^2 at 2.6 eV. Smaller structures are observed between 3 eV and 6.6 eV, with a maximum cross section never exceeding about 1.2×10^{-16} cm^2. All features are due to enhancement of the direct excitation *via* a multitude of narrow, closely-spaced resonances calculated by the theory, the effects of which are convoluted by the 125 meV energy resolution of the present experiment. Iron is present in practically every astrophysical object, as well as being an impurity in fusion plasmas. Present results are the highest charge state in any ion for which an absolute excitation cross section has been measured.

DOI: 10.1103/PhysRevA.75.022709 PACS number(s): 34.80.Dp, 97.10.Tk

I. INTRODUCTION

The $3s^23p\ ^2P^o_{1/2} - 3s^23p\ ^2P^o_{3/2}$ coronal green line (λ5303 Å) (2.338 eV) transition in Fe^{13+} is an important diagnostic of the solar corona [1–3]. Its abundance and brightness in the cool solar corona ($T=2\times10^6$ K) and in active regions ($T=4\times10^6$ K) has allowed one to use the green-line transition to map isointensity contours of the polar coronal and hole structure [4,5], and to map long-term changes in the coronal structure [6,7]. In general, the lines in $Fe^{8+}-Fe^{13+}$ are important diagnostics of ionization balance, electron temperature (T_e) and electron density (N_e) in different solar regions and features [8,9]. The $3s^23p\ ^2P^o_{1/2} - 3s^23p\ ^2P^o_{3/2}$ excitation rate also determines the density dependence of the allowed Fe^{13+} lines near λ200 Å observed by the EIS spectrometer aboard the Hinode satellite.

Coronal observations of Fe^{13+} apply to gas near 2×10^6 K. At that temperature, kT is ≈170 eV, so resonance structure near the 2.5 eV threshold is of modest importance. Moreover, there are strong contributions to the excitation rate from protons, and from excitations to allowed levels that cascade back to the upper state of the λ5303 Å transition [10]. The resonance structure near threshold is much more important in photoionized gas, where Fe^{13+} can be produced at temperatures $kT\approx10$ eV. Porquet *et al.* [11] show that Fe^{13+} formed in photoionized gas strongly constrains warm absorber models for AGN winds. The Fe^{13+} line is only seen in about one-fourth the Seyfert galaxies, and it is not yet clear whether it is formed in purely photoionized gas or in million-degree gas mixed in with the photoionized gas [12]. Ferguson *et al.* [12] also point out the importance of resonances in the cross sections, in particular the factor of ten differences between cross sections without resonances and the largest of the cross sections that include resonances. They find that if the cross sections with the largest resonance contributions are correct, Fe must be, implausibly, depleted by a similarly large factor relative to Mg, Si, and Ca.

In order to convert line intensities to actual T_e and N_e one needs both reliable theoretical and experimental data. For almost all ion species, and for practically all charge states and transitions, only theoretical data are available, with no comparison to absolute, or even normalized, experimental cross sections. Presented herein are first experimental measurements of absolute collisional excitation cross sections for the $^2P^o_{1/2}-^2P^o_{3/2}$ transition in Fe^{13+}. Comparison is given with new theoretical results in a 135-level Breit-Pauli *R*-matrix calculation for this transition.

The experimental measurements were carried using techniques similar to those used in absolute excitation measurements for the Fe^{9+} coronal red line [13]. The 14.0 GHz electron cyclotron resonance (ECR) ion source at the JPL Highly Charged Ion Facility was used, with the $^{56}Fe^{13+}$ ions generated from ferrocene vapor [dicyclopentadienyl iron, $Fe(C_5H_5)_2$], and extracted at 13×7.0 keV from the ECR source.

II. EXPERIMENTAL DETAILS

Experimental methods, and data acquisition and analysis methods may be found in Refs. [14–16]. The electron energy-loss method is used, together with merged beams of low-energy electrons and Fe^{13+} ions. The distribution of Fe^{q+} charge states from the ECR plasma is mass/charge analyzed in a double-focusing 90° bending magnet. The resolved Fe^{13+} beam is transported and focused into the interaction region where it is merged with a magnetically-confined electron beam using a trochoidal deflector. The electrons and ions interact, and the target excitation occurs along a 20.0±0.3 cm path length. The electrons are then demerged from the ions using a second trochoidal analyzer, and their spatial position and current are measured by a position-sensitive detector at the exit plane of the second trochoidal system. Electron and ion beam profiles are measured at four

TABLE I. Individual and total-quadrature experimental uncertainties in the e-Fe^{13+} cross sections, for a single measurement at a given energy.

Source of uncertainty	Uncertainty (1σ confidence level) (%)
Counting statistics	3.0
Form factor	6.0
Path length	1.0
Electron-current measurement	0.5
Ion-current measurement	0.5
PSD efficiency calibration	1.5
Overlapping elastic contribution	7.0
Metastable fraction	4.0
Total quadrature uncertainty (at 1.7σ or 90% CL)	18%

locations along the merged path using vanes with circular holes that intersect the merged beams at different radial distances. An electronic aperture [15] is used to discriminate against elastically-scattered electrons prior to the trochoidal electron energy-loss analyzer; and retarding grids are used after the analyzer. Small, remnant background signals from elastically-scattered electrons which may overlap the inelastic spectrum are accounted for through the use of trajectory modeling and calculated elastic differential cross sections. These three features, combined with the velocity dispersion of the trochoidal monochromator, allow one to carry out energy-loss measurements at energies from about $0.7\times$ threshold to approximately $3\times$ threshold.

The usual relation between experimentally measured quantities and the excitation cross section $\sigma(E)$ (cm^2) at a center-of-mass (c.m.) energy E is given by

$$\sigma(E) = \frac{\mathbb{R}qe^2\mathcal{F}}{\epsilon I_e I_i L}\left|\frac{v_e \cdot v_i}{v_e - v_i}\right|, \tag{1}$$

where $\mathbb{R}$ is the total signal rate (s^{-1}), q is the ion charge (dimensionless), e is the electron charge (C), I_e and I_i are the electron and ion currents (A) respectively, v_e and v_i are the electron and ion velocities ($cm\,s^{-1}$) respectively, L is the merged path length (cm), ε is the efficiency of the combined rejection-grid and microchannel-plate detection system (dimensionless), and $\mathcal{F}$ is the overlap factor between the electron and ion beams (cm^2).

All quantities in Eq. (1) are measured, or in the case of the particle velocities are known nominally through their acceleration potentials. Errors inherent to the quantities in Eq. (1) are discussed in Smith *et al.* [17], and individual errors are displayed in Table I. Knowledge of the fraction of Fe^{13+} ions in metastable states is important in that excitation events out of metastable levels are *not* counted in the rate $\mathbb{R}$, but the metastable current *is* counted in I_i. Use of the gas-beam attenuation method [18,19] to monitor the metastable-state fraction would not be reliable in this case. The Fe^{13+} charge exchange cross sections for ground and metastable states are expected to be nearly identical, and hence one does not expect to observe significant "breaks" in the slope of the attenuation curves. However, one is aided by an additional feature of the JPL beam lines. Using the Kingdon ion trap beam line, metastable lifetimes of Fe^{9+}, Fe^{10+}, and Fe^{13+} were recently reported [20]. In the case of the Fe^{13+} lifetime, the λ5303 Å photon was observed as the ions decayed in the $^2P^o_{3/2}$–$^2P^o_{1/2}$ M1 transition, the $^2P^o_{3/2}$ level having been excited within the plasma of the ECR source. This emission served as a convenient diagnostic for the effect of the ECR operating parameters on the metastable ion current. It was readily apparent that the greatest photon yield, and hence the greatest metastable $^2P^o_{3/2}$ population, occurred when the ECR was operated at a low ferrocene pressure (10^{-5} Pa, as measured just external to the ECR plasma chamber). When the ferrocene vapor pressure was increased above $\approx 4\times 10^{-5}$ Pa the photon signal was weak or absent, presumably due to a large quenching rate of the metastable level. To augment this collisional quenching effect, it was found that a constant flow of either Ar or N_2 at $\approx 7\times 10^{-5}$ Pa (admitted into the plasma chamber through an alternate side port) also gave a negligible photon decay rate.

Naturally, there is ion charge-state loss due to charge exchange to Fe^{q+} ($q<13$) within the plasma, but several nA currents of Fe^{13+} could still be maintained. Therefore in all runs the ECR was operated with a gas buffer load. The coronal green line emission intensity was monitored over several weeks, at the same time that the Fe^{13+} lifetimes were being measured. Finally, similar metastable quenching results have been observed with Fe^{11+} and S^{5+} beams, and these results will be discussed in a separate report.

As to the error estimate due to elastic electron scattering, since this scattering scales as the square of the ion charge, it is 169 times more intense for Fe^{13+} than for O^+, for example. The error in the elastic scattering background (7.0%) is determined by the ability of the electronic aperture to reject the larger Larmor-radius electrons, the ability of the retarding grids to reject forward-scattered electrons, and the estimated error incurred in modeling the remaining high angle, elastically-scattered electrons using angular distributions from phase-shift calculations [17]. The error in measurements *below* threshold is a conservative estimate of the error encountered in subtracting a small, residual elastic contribution to the total inelastic scattering. The error bars on the final data represent 1–5 independent measurements at each c.m. energy.

The electron energy scale was calibrated at several times by use of retarding potential difference method with the grids

TABLE II. Comparison of the present calculated level energies (eV) with spectroscopically-determined values. The latter are available at the NIST website http://physics.nist.gov.

Index	Term	J	Theory (T)	Spectroscopic (S)	δ (%) $[(1-\mathrm{T/S})\times 100]$
1	$3s^2 3p\ ^2P^o$	1/2	0.00	0.00	0.0
2		3/2	2.18	2.34	6.8
3	$3s3p^2\ ^4P$	1/2	27.53	27.91	1.4
4		3/2	28.40	28.86	1.6
5		5/2	29.53	30.05	1.7
6	$3s3p^2\ ^2D$	3/2	37.09	37.10	0.03
7		5/2	37.33	37.38	0.01
8	$3s3p^2\ ^2S$	1/2	45.59	45.22	−0.8
9	$3s3p^2\ ^2P$	1/2	48.68	48.17	−1.1
10		3/2	49.69	49.16	−1.1
11	$3s^2 3d\ ^2D$	3/2	59.86	58.67	−0.3
12		5/2	60.13	58.92	−2.1
13	$3p^3\ ^2D^o$	3/2	71.21	71.46	0.3
14		5/2	71.62	71.94	0.04
15	$3p^3\ ^4S^o$	3/2	72.89	73.03	0.02
16	$3p^3\ ^2P^o$	1/2	79.75	79.64	0.2
17		3/2	79.77	80.02	0.3
18	$3s3p3d\ ^4F^o$	3/2	80.09	–	–
19		5/2	80.24	80.09	−0.2
20		7/2	80.93	80.83	−0.1
21		9/2	81.88	81.86	−0.02

in front of the position-sensitive detector (PSD). A constant 1.0±0.1 V offset was measured between the nominal cathode bias voltage and the grids cutoff voltage. In addition, experimental excitation thresholds for transitions in Fe^{11+} and S^{5+} were also used for calibaration. The offset as measured with the retarding grids, together with the spectroscopic energy-onset of the signal were used to fix the energy scale with a 0.1 eV error. The resolution of the electron beam (125 meV, FWHM) was comparable to that in previous measurements.

III. THEORETICAL AND COMPUTATIONAL DETAILS

Included in the full Breit-Pauli *R*-matrix calculation is a total of 135 fine-structure levels arising from 59 LS terms of the $3s^2 3p$, $3s3p^2$, $3p^3$, $3s^2 3d$, $3s3p3d$, $3s3d^2$, $3p3d^2$, $3p^2 3d$, $3s^2 4s$, $3s^2 4p$, and $3s^2 4d$ configurations. These levels have been represented by configuration-interaction wave functions that are constructed by spectroscopic and correlation orbitals. Accurate description of target wave functions is an essential part of a reliable collision calculation. The wave-function calculation has been carried out using the multiconfiguration Hartree-Fock method and accompanying codes [21]. In this approach each atomic state is represented by an atomic state function written as an expansion of the configuration state functions. These are constructed from one-electron 1*s*, 2*s*, 2*p*, 3*s*,3*p*, 3*d*, 4*s*, 4*p*, 4*d*, and 4*f* radial functions. Relativistic effects are allowed by means of the Breit-Pauli operators; and the *J*-dependent atomic state functions are written as a sum over different LS values, which couple to give the total angular momentum *J*. The quality of target wave functions was assessed by comparing computed excitation energies and oscillator strengths with experimental values and other calculations. A comparison between present calculations and spectroscopic results for the lowest 21 levels is given in Table II. One sees that the calculated values of 19 energy levels agree with spectroscopic values [22] to better than 1% on average.

The total wave function representing the collision of electrons with Fe^{13+} for each total angular momentum *J* and parity π is expanded in the *R*-matrix basis [23]

$$\Psi_k = A\sum_{ij} a_{ijk}\bar{\Phi}_i u_j(r) + \sum_j b_{jk}\phi_j, \tag{2}$$

where $\bar{\Phi}_i$ are channel functions formed from the multiconfigurational functions of the 135 target levels that are included in the close-coupling expansion, and u_j are the radial basis functions describing the motion of the scattering electron. The operator *A* antisymmeterizes the wave functions and a_{ijk} and b_{jk} are expansion coefficients determined by diagonalizing the $(N+1)$-electron Hamiltonian, performed once for the entire range of scattering calculation energies. Included were 18 continuum orbitals for each total angular momentum *J* to obtain convergence for the incident electron energies. Sufficient numbers of $(N+1)$-electron bound con-

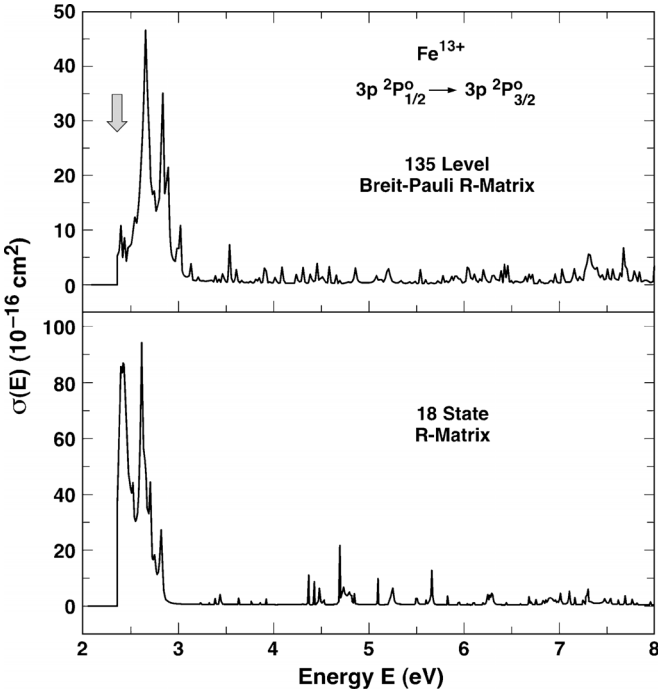

FIG. 1. Calculated excitation cross sections for the coronal green line transition in the present 135-level *R*-matrix formulation (upper panel), and in the 18-state *R*-matrix approach [3] (lower panel). The vertical arrow here and in Fig. 2 denotes the spectroscopic threshold for the transition at 2.34 eV. Results have been shifted by 0.16 V (upper) and 2.34 eV (lower) to agree with the established threshold energy.

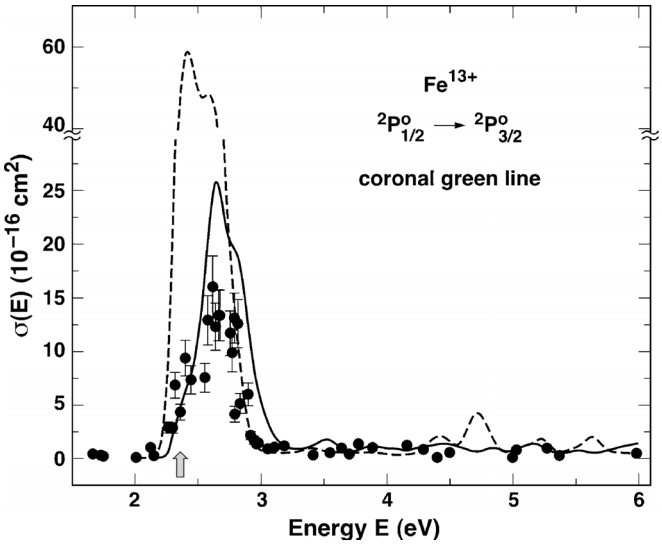

FIG. 2. Comparison of the convoluted 135-level Breit-Pauli *R*-matrix results (solid line, present results) and 18-state *R*-matrix results (dashed line) [3] with measured absolute experimental cross sections (solid circles) for the $3s^2 3p\ ^2P^o_{1/2} - 3s^2 3p\ ^2P^o_{3/2}$ transition in Fe^{13+}. Experimental errors are given at the $1.7\sigma(90\%)$ confidence level. This is 18% or less, depending on the number of measurements (1–5) of each cross section.

figurations were included in the second expansion to allow for important short-range correlations. The functions N_j are bound-state type included to allow for short-range correlation effects. The partial collision strengths have been calculated for J values from 0 to 25. The collision calculation was carried out at a very fine energy mesh of 0.0001 eV to delineate the resonance structures. These structures are complex and make substantial enhancements to the cross section.

IV. RESULTS AND DISCUSSION

As in the case of the Fe^{9+} coronal red line, the green line excitation is dominated by resonances at threshold. These resonances are too narrow to be resolved with the present experimental resolution, and hence the displayed, calculated results are the cross section averaged over these sharp structures. An expression for the c.m. energy E in terms of the laboratory energies E_e and E_i of electrons and ions, respectively, is given in Eq. (2) of Ref. [13]; and the corresponding equation for calculating the behavior of the energy resolution in the c.m. as a function of the laboratory electron energy E_e is given in Eq. (3) of that publication.

Results of the 135-level Breit-Pauli *R*-matrix calculation are shown in Fig. 1, along with results of the 18-state *R*-matrix calculation of Ref. [3]. Both theories have been shifted in energy to correspond to the spectroscopic threshold of 2.34 eV for the $^2P^o_{1/2} - ^2P^o_{3/2}$ transition. These shifts were 0.16 eV and 2.34 eV to the high-energy side for the present results and the 18-state results, respectively. (The larger shift in the 18-state results is because of the use of LS coupling, and hence the neglect of the energy splitting of the $^2P^o$ fine structure levels.) Each theory reveals a rich threshold resonance structure. The locations of the resonances are slightly different, and the 18-state cross section results are approximately a factor of two larger than those of the 135-level calculation. The 18-state *R*-matrix calculation in Ref. [3] was performed in LS coupling by including the Darwin and mass Breit-Pauli operators in the scattering calculation. An algebraic transformation was then used to obtain fine-structure collision strength. The effects of intermediate coupling were considered through the use of the term coupling coefficients [24]. This approach has two main limitations compared to a full Breit-Pauli *R*-matrix calculation. The fine-structure splitting of the target terms is neglected, and in the resonance region, where there are both open and closed channels, only those components of the term coupling coefficients are used for which channels are open. Both of these approximations may have caused significant inaccuracies in the 18-state calculation for Fe^{13+}, for which the spin-orbit interaction is important. The discrepancies between the two calculations may also have been caused by the differences in target wave functions.

To compare with experiment, both sets of theoretical results were convoluted with the electron energy-dependent resolution of the experiment. A measured electron energy resolution of $\Delta E_e = 125$ meV was used. The convoluted results of both theories are shown along with the presentexperimental results in Fig. 2. The measured cross sections

TABLE III. Experimental cross sections for the $3s^2 3p\ ^2P^o_{1/2} - 3s^2 3p\ ^2P^o_{3/2}$ transition in Fe^{13+}. The experimental error is 18% (90% CL) or less, depending on the number of measurements at each energy. The excitation threshold is 2.34 eV.

Energy E (eV)	Cross section $\sigma(E)(10^{-16}$ cm$^2)$
1.67	0.34
1.73	0.23
1.75	0.14
2.01	0.01
2.12	0.94
2.15	0.17
2.27	2.83
2.30	2.81
2.32	6.76
2.36	4.24
2.40	9.28
2.45	7.27
2.58	12.8
2.56	7.47
2.62	15.9
2.64	12.2
2.67	13.3
2.76	11.6
2.77	9.79
2.79	13.0
2.80	4.06
2.82	12.5
2.84	5.06
2.90	5.92
2.92	2.07
2.95	1.57
2.97	1.27
2.98	1.34
3.06	0.81
3.11	0.99
3.19	1.10
3.42	0.22
3.55	0.46
3.64	0.87
3.70	0.33
3.78	1.29
3.89	0.92
4.16	1.14
4.29	0.78
4.40	0.03
4.50	0.48
5.00	0.02
5.03	0.68
5.27	0.87
5.37	0.21
5.98	0.39
6.40	0.24
6.62	0.76

and the c.m. energy are listed in Table III. The convolution has averaged the sharp threshold resonances into a broader peak centered at 2.4 eV (18 state) and 2.6 eV (135 level). It is seen that experiment and theories confirm the strong resonances at threshold. The measured peak of 2.7 ± 0.1 eV is in good agreement with the theoretical range 2.4–2.6 eV, considering the error in experimental energy scale and uncertainty in the location of the maximum cross section. In addition there are theoretical uncertainties due to the type and number of bound and continuum orbitals, and the description of electron correlation and relativistic effects. As noted earlier [13] differences of the order of 0.2 eV (0.015 Ry) have a negligible effect on the effective collision strengths often used in astrophysics, as collision strengths involve integration over a large energy interval. There is also evidence in the experimental data and both theoretical results of the weaker shoulder at 2.6 eV (18 state) and 2.8 eV (135 level and experiment).

The results of Ref. [3] are higher than both experiment and present calculation. One sees that the peak of the energy-convoluted 18-state cross sections [3] is a factor of 4.2 above experiment; and a factor 2.4 above the present calculation. This difference is consistent with the discrepancy in the iron abundance in Seyfert Galaxies (the so-called "Iron Conundrum") [12]. The results of Ref. [3] gave an (improbable) under-abundance of the Fe density (relative to that of Mg, Si, Ca, etc.) by a factor of about ten relative to solar abundances. The present experimental data, supported by the 135-level results, would predict an iron abundance that is now about a factor of 2.4 below solar, which is more reasonable.

The present results represent the first experimental data on excitation cross sections in Fe^{13+}, and the highest charge state for which an absolute excitation cross section has been measured. Iron is present throughout the universe, in stars, our Sun, and in the interstellar medium. It is also a significant impurity in high-electron temperature plasmas such as the tokamak, the Joint European Torus, and the upcoming International Thermonuclear Experimental Reactor (ITER). As such, the present experimental and theoretical approach is directed to measuring absolute excitation cross sections for low-lying transitions in a Fe charge states up to the limit of the ECR production (14+ to 16+), covering the c.m. energy range from threshold to approximately $3-5\times$ the threshold energy.

ACKNOWLEDGMENTS

S.H. thanks the National Academy of Science-National Research Council and the NASA Postdoctoral Program for support. S.S.T. is supported by NASA under Grant No. NNG06GD39G from the Astronomy and Physics Research Analysis Program. The experimental work was carried out at the Jet Propulsion Laboratory, California Institute of Technology, and was supported under contract with NASA.

[1] M. Arnaud and J. C. Raymond, Astrophys. J. **398**, 394 (1992).
[2] H. E. Mason, At. Data Nucl. Data Tables **57**, 305 (1994).
[3] P. J. Storey, H. E. Mason, and P. R. Young, Astron. Astrophys., Suppl. Ser. **141**, 285 (2000).
[4] Y.-M. Wang *et al.*, Astrophys. J. **485**, 419 (1997).
[5] E. C. Roelof, G. M. Simnett, R. B. Decker, L. J. Lanzerotti, C. G. Maclennan, T. P. Armstrong, and R. E. Gold, J. Geophys. Res. **102**, (A6), 11251 (1997).
[6] O. G. Badalyan and V. N. Obridko, Astron. Rep. **48**, 678 (2004).
[7] V. I. Makarov and A. G. Tlatov, Astron. Rep. **49**, 932 (2005).
[8] N. S. Brickhouse, J. C. Raymond, and B. W. Smith, Astron. Astrophys., Suppl. Ser. **97**, 551 (1995).
[9] A. Chutjian, Phys. Scr. **T110**, 203 (2004).
[10] H. Nussbaumer and D. E. Osterbrock, Astrophys. J. **161**, 811 (1970).
[11] D. Porquet, A.-M. Dumont, S. Collin, and M. Mouchet, Astron. Astrophys. **341**, 58 (1999).
[12] J. W. Ferguson, K. T. Korista, and G. J. Ferland, Astron. Astrophys., Suppl. Ser. **110**, 287 (1997).
[13] M. Niimura, I. Čadež, S. J. Smith, and A. Chutjian, Phys. Rev. Lett. **88**, 103201 (2002).
[14] A. Chutjian, J. B. Greenwood, and S. J. Smith, in AIP Conf. Proc. No. 475, Applications of Accelerators in Research and Industry, edited by J. L. Duggan and I. L. Morgan (AIP, Woodbury, 1999).
[15] J. B. Greenwood, S. J. Smith, A. Chutjian, and E. Pollack, Phys. Rev. A **59**, 1348 (1999).
[16] S. J. Smith, N. Djurič, J. A. Lozano, K. A. Berrington, and A. Chutjian, Astrophys. J. **630**, 1213 (2004).
[17] S. J. Smith, J. B. Greenwood, A. Chutjian, and S. S. Tayal, Astrophys. J. **541**, 501 (2000).
[18] C. Liao, S. J. Smith, D. Hitz, A. Chutjian, and S. S. Tayal, Astrophys. J. **484**, 979 (1997).
[19] S. J. Smith, M. Zuo, A. Chutjian, S. S. Tayal, and I. D. Williams, Astrophys. J. **463**, 808 (1996).
[20] S. J. Smith, A. Chutjian, and J. A. Lozano, Phys. Rev. A **72**, 062504 (2005).
[21] O. Zatsarinny and C. Froese Fischer, Comput. Phys. Commun. **124**, 247 (2000).
[22] Spectroscopic data are available at the website http://physics.nist.gov
[23] K. A. Berrington, W. B. Eissner, and P. H. Norrington, Comput. Phys. Commun. **92**, 290 (1995).
[24] H. E. Saraph, Comput. Phys. Commun. **15**, 247 (1978).